Measuring Flow Angle and Mass Flow Rate in an Unknown Flowfield

Vernon T. Helms III*
NASA Langley Research Center, Hampton, Va.

A data reduction technique applicable to constant-temperature hot-film and hot-wire probes is presented which is used to determine flow angle and mass flow rate in an unknown flowfield over a wide range of flow conditions at supersonic and hypersonic velocities. The technique virtually eliminates the effect of Reynolds number on a probe's flow angle sensitivity. Methods for extrapolating a limited amount of mass flow rate calibration data to include the range of mass flow rate encountered in an experiment are also given. This technique has been applied to data obtained using a hot-film probe during surveys in the leeside flowfield of a Space Shuttle Orbiter configuration.

Nomenclature

A' = term in Nusselt number equation which includes the effect of heat convection at zero velocity and end losses for heated cylinders
B = constant in the equation for Nusselt number
b = maximum spanwise dimension of model
d = diameter of sensor
$f(\theta,\alpha)$ = general relation defined in Eq. (12)
I = current measured in sensors
K_1, K_2 = experimentally determined quantites which minimize the effect of Reynolds number on the flow angle calibration of a hot-film or hot-wire probe
k = thermal conductivity of test medium
L = length of model
l = length of sensing element on a hot-film or hot-wire probe
M = Mach number
n = exponent of Reynolds number in the equation for Nusselt number
Nu = Nusselt number
P = pressure
R = resistance of a hot-film or hot-wire sensor; if used without a subscript, it is the resistance at the sensor's operating conditions
Re = Reynolds number
S = coefficient of heat transfer between a hot-film or hot-wire sensor and the flow due to forced convection defined in Eqs. (2) and (3)
T = temperature
ΔT = difference between the sensor and the recovery temperature
u = flow velocity
u_{eff} = effective cooling velocity
x = axial distance on model measured from nose
y = semispan distance on model measured from symmetry plane
Z = distance along a survey path measured in a direction perpendicular to the freestream
α = angle of attack
β = sideslip angle of probe
δ = numerator of Eq. (6)
θ = angle between a sensor and the probe's reference line
μ = viscosity
ρ = flow density
ϕ = flow angle calibration parameter
ψ = mass flow rate calibration parameter

Subscripts

1 = conditions for sensor 1 except when used with K_1
2 = conditions for sensor 2 except when used with K_2
c = quantities measured at room temperature
l = local flow conditions
n = normal to a sensor's axis
0 = stagnation values
r = recovery
t = total
∞ = freestream
exp = experimental value
cal = calibration value

Introduction

PREVIOUS data reduction techniques used to determine flow angle and other properties with dual-element hot-film and hot-wire probes require that the calibration and tests be conducted with approximately the same flow conditions, or that the physical and electrical characteristics of the individual sensors be precisely matched and details of probe construction and material properties be known. The new data reduction technique presented in this paper is an improvement over the previous methods. It allows flow angle and mass flow rate to be determined in a completely unknown flowfield over a wide range of conditions at both supersonic and hypersonic velocities. Reasonably close correspondence of sensor characteristics is always desirable, but the present method does not require precisely matched sensors or specific knowledge of probe construction and material properties. However, it does require that calibrations be made over a wide enough range of flow conditions to establish trends in the calibration curves. A method will be presented which uses these trends to formulate an extrapolation that allows accurate measurement of experimental mass flow rates that are beyond the range of the calibrations.

The new data reduction technique has been applied to measurements obtained using a hot-film probe during surveys in the leeside flowfield of an early version of the Space Shuttle Orbiter at Mach 20.3 in helium. The purpose of this investigation was to determine if leeside flow models developed from studies of oil flow patterns and heating contours adequately describe structures in the flowfield away from the model's surface. This study revealed some unexpected flow patterns in the separated region above the wing.

Presented as Paper 78-794 at the AIAA 10th Aerodynamic Testing Conference, San Diego, Calif., April 19-21, 1978; submitted May 24, 1978; revision received Sept. 20, 1978.

Index category: Supersonic and Hypersonic Flow

*Aerospace Engineer, Aerothermodynamics Branch, Space Systems Division.

Table 1 Flow properties for hot-film probe calibrations and symbols used on the calibration curves.

Facility	P_0, 10^6 N/m^2	M_∞	$R_{e,\infty}$, 10^6 m^{-1}	$(\rho u)_\infty$, kg/m^2-s	α, deg	β, deg	Symbol
22-in. helium tunnel	6.897	20.3	21.49	12.248	−30-+30	0	○
						10	●
						20	×
	3.449	19.1	11.10	7.276		0	□
Low Reynolds number helium tunnel	0.080	3.94	2.20	13.839	−12-+12	0	◇
	0.027	3.77	0.78	5.119		0	△
	0.007	3.33	0.24	1.742		0	▷

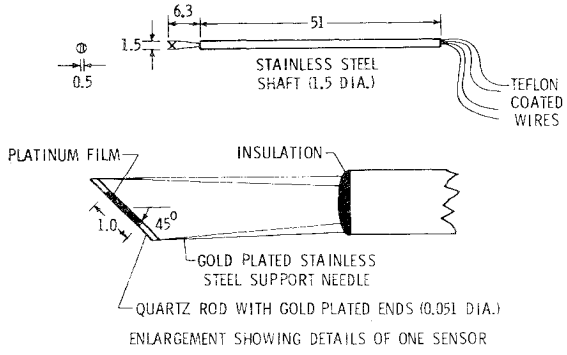

Fig. 1 Sketch of hot-film probe; all dimensions are in millimeters.

Hot-Film Probe

The methods described herein can be used with either constant temperature hot-film or hot-wire probes with dual sensors. The calibration of a hot-film probe was used to evaluate the new data reduction technique. A diagram of the probe is given in Fig. 1. It consists of two mutually perpendicular sensors separated by a very small distance with each one attached to the ends of gold-plated stainless steel support needles. The sensing element is a thin platinum film deposited onto a cylindrical quartz rod with gold-plated ends. The gold plating isolates the platinum film and provides a metallic contact between the sensor and its supports. The base of each support needle is anchored into an insulating material at the end of the probe's stainless steel shaft. Teflon-coated wires that are connected to the needles carry the signal from a two-channel constant temperature anemometer.

Probe Calibration

The hot-film probe was calibrated over a wide range of flow conditions in both the Langley 22-in. helium tunnel and a low Reynolds number helium tunnel, as shown in Table 1. The freestream Reynolds number for these calibrations based on a sensor diameter of 0.051 mm varied from 12-1105. The symbols given in this table correspond to those used in graphs that will be presented later. The characteristics of the 22-in. tunnel's test section can be found in Ref. 1 and those of the low Reynolds number tunnel in Ref. 2. The low Reynolds number tunnel was designed and built specifically for probe calibration.† The range in angle of attack was limited to ±12 deg in the low Reynolds number tunnel, but the calibration was extended to ± 30 deg in the 22-in. tunnel. The probe's calibration consisted of recording several seconds of data on magnetic tape with the desired freestream conditions at intervals between the limits in angle of attack permitted by the facility. Two measurements at each angle of attack were made to insure greater accuracy and repeatability. Additional information on test procedures and equipment is available in Ref. 3.

†Design, construction, and initial testing of the low Reynolds number tunnel was supervised by L.M. Weinstein, Fluid Mechanics Branch, Langley Research Center.

Data Reduction

Flow Angle Measurements

Making flow angle measurements in an environment where a variety of flow conditions can be expected requires that a single calibration curve define the probe's flow angle sensitivity over a wide range of conditions. The standard form of the flow angle calibration parameter used in many investigations where calibration and test conditions are nearly the same is not suitable for this purpose because it has no provisions for removing the effects of variable flow properties, which is basically a Reynolds number effect. This form of the flow angle calibration parameter is

$$\phi = (S_1 - S_2)/(S_1 + S_2) \tag{1}$$

The terms S_1 and S_2 are heat-transfer coefficients which equate heat lost from the surface of the cylindrical sensors to the flow due to forced convection and are defined as

$$S_1 = I_1^2 R_1/(T_1 - T_r) \tag{2}$$

and

$$S_2 = I_2^2 R_2/(T_2 - T_r) \tag{3}$$

The stagnation temperature in both wind tunnels was approximately equal to room temperature. The sensor temperatures T_1 and T_2 were set at 25% above room temperature and are of the form[4]

$$T = T_c R/R_c \tag{4}$$

The recovery temperature was selected as the reference temperature for this study, although several forms of reference temperature are in common use.[5] It has been shown[4] that the recovery temperature for cylinders in high-speed helium flow can be expressed as

$$T_r = 0.96\ T_{t,\infty} \tag{5}$$

Plots of ϕ vs α using Eq. (1) for various flow conditions would result in curves which have different values of ϕ and different slopes at a given angle of attack.

The influence of variable flow properties can be minimized by modifying the standard flow angle calibration parameter to the form‡

$$\phi = (K_1 S_1 - S_2)/(K_1 S_1 + S_2 - K_2) \tag{6}$$

The quantities K_1 and K_2 are determined experimentally and are related to the ratio of cold resistance for the two sensors and the sum of the no-flow heat losses of the two films, respectively. Using these constants provides a method of correlating a probe's response to flow angularity over an extremely wide range in flow conditions. This can be proven by first considering the equation for Nusselt number[6]:

$$Nu = I^2 R/\pi l dk \Delta T \tag{7}$$

‡Suggested by L.M. Weinstein.

which equates heat lost to the flow with electrical power required to maintain the cylindrical sensors at a constant temperature. The temperature difference term is defined as

$$\Delta T = T - T_r \tag{8}$$

Nusselt number for heated cylinders in flow was expressed by King[7] as

$$Nu = A' + BRe^n \tag{9}$$

With the equation in this form, the quantity A' contains the effect of end losses and heat lost due to convection at zero velocity. End losses for hot-film probes arise from heat conducted away from the platinum film and into the quartz rod and the support needles. In the case of hot-wire probes, heat is conducted directly from each wire into its support needles. End losses depend on Reynolds number as well as other variables such as sensor geometry, material properties, probe construction, and the difference between the reference and the sensor temperatures. The exponent n varies from approximately 0.5 for continuum flow to 1.0 for free molecular flow.[6] It has been shown to be constant at approximately 0.72 for hot wires over a wide range of conditions in high-speed helium flow.[4] The quantity B has a mild dependence on flow properties, but over a reasonably small range of temperature it can be considered constant.[6] The effects of radiation would be of importance to the overall response of the probe only at very low densities; but because of the relatively low operating temperature of the sensors in the present study, end losses are the dominant effect in low-density flow. Therefore, radiation is not accounted for in these equations. It is generally assumed that hot-film and hot-wire sensors obey King's law, Eq. (9), so that

$$I^2R/\pi ldk\Delta T = A' + BRe^n \tag{10}$$

Applying the definition of the parameter S from Eqs. (2) and (3), Eq. (10) becomes

$$S/\pi ldk = A' + B(\rho u_{\text{eff}} d/\mu_{t,\infty})^n \tag{11}$$

The velocity in the Reynolds number term is the effective cooling velocity. To a first approximation it can be considered as the component of velocity normal to the axis of a sensor and is governed by a sine law as shown in Fig. 2. More accurate expressions which account for the effects of induced flow parallel to a sensor's axis at angle of attack[8] and for pitch and yaw factors[9] have been formulated. These relations depend only upon sensor geometry, which is constant for each probe and angle of attack. For the purpose of the present discussion, the effective cooling velocity need only be expressed as general function given by

$$u_{\text{eff}} = u\, f(\theta,\alpha) \tag{12}$$

where u is the total velocity ahead of the probe and θ is the angle between the sensor's axis and the probe's reference line, usually the axis of the shaft. The quantity ρu_{eff} in Eq. (11) is the freestream mass flow rate during calibration of the probe and it is the local value during the survey of an unknown flowfield. Viscosity is calculated using total temperature because most of the heat transferred to the flow takes place in the subsonic flow region on the front part of the sensor near stagnation conditions.[6] Equation (11) for both sensors can now be written as

$$S_1 = A_1 + B_1(\rho u)^n f_1^n(\theta_1,\alpha) \tag{13}$$

$$S_2 = A_2 + B_2(\rho u)^n f_2^n(\theta_2,\alpha) \tag{14}$$

where

$$A_1 = \pi l_1 d_1 kA' \tag{15}$$

$$A_2 = \pi l_2 d_2 kA' \tag{16}$$

$$B_1 = \pi l_1 d_1 kB(d_1/\mu_{t,\infty})^n \tag{17}$$

$$B_2 = \pi l_2 d_2 kB(d_2/\mu_{t,\infty})^n \tag{18}$$

Substituting Eqs. (13) and (14) into Eq. (6) yields the expression

$$\phi = \frac{K_1A_1 + K_1B_1(\rho u)^n f_1^n(\theta_1,\alpha) - A_2 - B_2(\rho u)^n f_2^n(\theta_2,\alpha)}{K_1A_1 + K_1B_1(\rho u)^n f_1^n(\theta_1,\alpha) + A_2 + B_2(\rho u)^n f_2^n(\theta_2,\alpha) - K_2} \tag{19}$$

The terms K_1A_1, A_2 and $(\rho u)^n$ contain the major influence of variable flow properties on the flow angle calibration parameter. The effect of these quantities can be virtually eliminated by choosing K_1 and K_2 such that

$$K_1A_1 \approx A_2 \tag{20}$$

and

$$K_2 \approx K_1A_1 + A_2 \tag{21}$$

Equation (20) is an approximation because A_1 and A_2 are Reynolds number dependent and, in general, cannot be made equal by a single constant. A similar argument holds for Eq. (21). The quantities K_1 and K_2 are experimental values that most closely satisfy these conditions so that the equation for ϕ becomes

$$\phi = \frac{K_1B_1f_1^n(\theta_1,\alpha) - B_2f_2^n(\theta_2,\alpha)}{K_1B_1f_1^n(\theta_1,\alpha) + B_2f_2^n(\theta_2,\alpha)} \tag{22}$$

which is primarily a function of angle of attack. Because S_1 and S_2, the heat transfer coefficients, depend upon the measured current and voltage in each sensor, ϕ can be calculated using Eq. (6) without knowing the value of A', B, n, f, dimensions and material properties of the sensors, or the probe's geometry.

The values of K_1 and K_2 are determined by an iterative process. This is illustrated in Fig. 3 which uses a portion of the hot-film probe's calibration data at three different flow conditions to show the flow angle calibration parameter plotted as a function of angle of attack for different values of K_1 and K_2. Arbitrary values can initially be assigned to K_1 and K_2 during data reduction. If $K_1 = 1$ and $K_2 = 0$, the flow angle calibration parameter is reduced to the standard form given by Eq. (1). The Reynolds number dependence of this expression is evident in the different values of ϕ and different slopes that the curves for various flow conditions have at a given angle of attack. The first step in determining the correct values of K_1 and K_2 is to hold K_1 constant while iterating for the value of K_2, which gives the same slope to the data curves for all calibration conditions. Then K_2 is held fixed while different values are substituted for K_1 until all of the data curves collapse as closely as possible to a single curve of ϕ vs α. For the hot-film probe used in this study, $K_1 = 0.96$ and $K_2 = 32$. Figure 4 shows the complete flow angle calibration of the hot-film probe. It includes data which cover a 60-deg range in angle of attack, a 90-to-1 range in Reynolds number, and Mach numbers from approximately 3-20. The probe is relatively insensitive to sideslip for angles as large as 20 deg. The modified flow angle calibration parameter was able to collapse the calibration data to within a very narrow band.

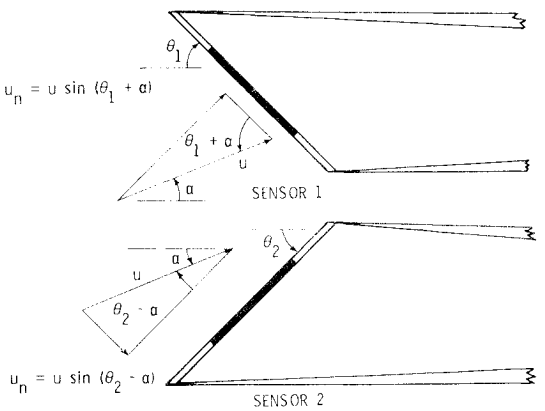

Fig. 2 Velocity components normal to hot-film sensors.

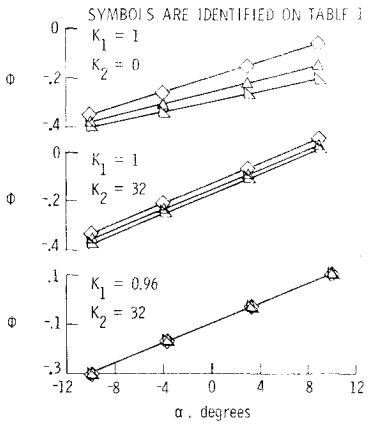

Fig. 3 Determining K_1 and K_2 for hot-film probe.

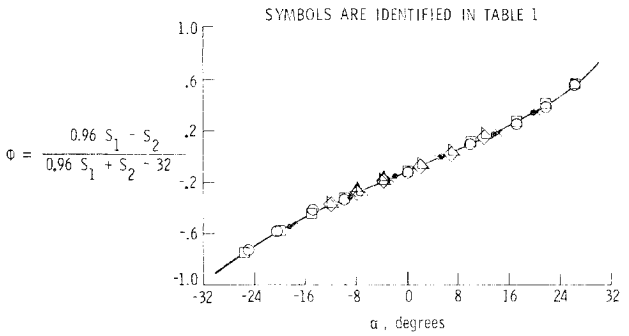

Fig. 4 Flow angle calibration of hot-film probe.

Mass Flow Rate Measurements

Both the numerator and denominator of Eq. (19) depend on mass flow rate, but only the denominator is a suitable mass flow rate calibration parameter. The numerator is defined as

$$\delta = [K_1 B_1 f_1^n(\theta_1,\alpha) - B_2 f_2^n(\theta_2,\alpha)]\,(\rho u)^n \tag{23}$$

or from Eq. (6) as

$$\delta = K_1 S_1 - S_2 \tag{24}$$

and cannot be used as a mass flow rate calibration parameter because at some angle of attack, which depends on the geometry and the value of K_1 for each probe, the term in brackets goes to zero and $\delta = 0$ for all values of ρu. This is illustrated in Fig. 5 where curves of δ vs α are presented using the calibration data of the hot-film probe. In this case, the angle at which $\delta = 0$ and the mass flow rate becomes indeterminant is approximately +5.6 deg. Interpolation between these curves would be very inaccurate with the probe at angles of attack with respect to the flow within several degrees of this value. The "zero point" of a calibration using Eq. (24) will generally fall within the angle-of-attack range of interest, making δ practically unusable as a mass flow rate indicator in an unknown flowfield.

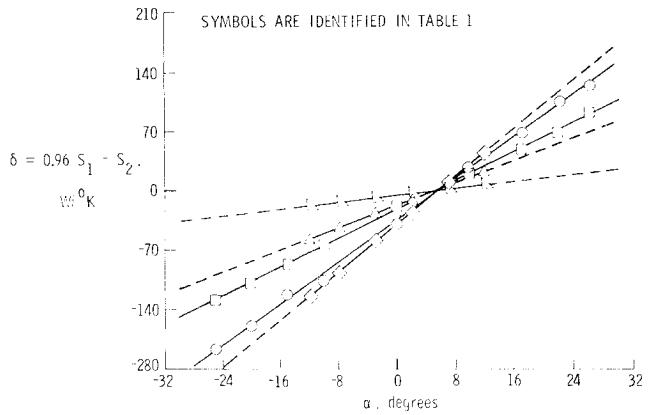

Fig. 5 Fictitious mass flow rate calibration using δ.

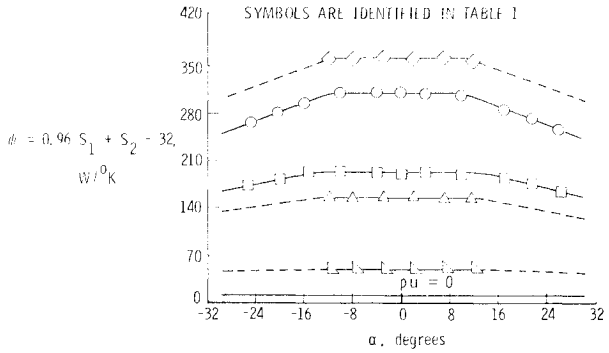

Fig. 6 Mass flow rate calibration of hot-film probe.

The denominator of Eq. (19) is defined as

$$\psi = [K_1 B_1 f_1^n(\theta_1,\alpha) + B_2 f_2^n(\theta_2,\alpha)]\,(\rho u)^n \tag{25}$$

The term in brackets is nearly constant over a wide range in angle of attack that is roughly centered at $\alpha = 0$ deg. This is due to the sine variation of the effective cooling velocity being approximately linear for a band of angles near 45 deg, which is very close to the value of θ_1 and θ_2 for the type of probe used in this study. As the term representing the response of one sensor increases, the other decreases by an almost equal amount. At extreme angles the sine law is no longer linear and ψ, for a given value of ρu, decreases with angle of attack. From Eq. (6), the mass flow rate calibration parameter can be written as

$$\psi = K_1 S_1 + S_2 - K_2 \tag{26}$$

so that, as with ϕ, it is determined from the measured current and voltage in each sensor. The freestream conditions in which the hot-film probe is calibrated for flow angle sensitivity represent different values of mass flow rate. By using Eq. (26) and plotting ψ vs α for each mass flow rate a set of curves is generated, as shown in Fig. 6. The mass flow rate in an unknown flowfield can be determined by interpolation, after first calculating ϕ from Eq. (6) and obtaining α from the calibration of ϕ vs α. The baseline in Fig. 6 represents the measured value of ψ at zero mass flow rate. It is a function of end losses and heat lost due to convection at zero velocity. These effects are contained in the quantity A' in Eq. (9).

Extrapolation of Mass Flow Rate Calibration to Higher Angles of Attack

The data for mass flow rate calibrations in the low Reynolds number tunnel were limited to angles of attack between ±12 deg. An extrapolation was applied to the mass flow rate calibrations, as shown by the dashed lines in Fig. 6, which extended these calibrations to angles of attack between ±30 deg. The basis for this extrapolation is to be found in Eq. (25). The value of ψ at different flow conditions can be related by a ratio of expressions, each in the form of Eq. (25) with the appropriate values of ρu and n for those conditions. The exponent n will vary slightly for different flow properties, but it is constant at a specified condition, which means that the ratio of the mass flow rate terms will be constant. The bracketed term in each expression also depends on n, but for a given set of flow properties, this term varies only with angle of attack, which means that the ratio of the bracketed terms is, at most, a weak function of n and can be considered constant. This implies that the ratio of mass flow rate calibration parameters for two different flow conditions is constant over the entire range in the probe's angle of attack. This result was verified using the curves of ψ vs α obtained in the 22-in. helium tunnel where calibrations were carried out over a 60 deg range angle of attack. These curves were used to extrapolate values of ψ for the low Reynolds number tunnel data by finding the ratio of mass flow rate parameters over the common angle-of-attack range. This procedure can only be used in a calibration where data have been measured over the entire angle-of-attack range of interest for at least one value of mass flow rate.

Extrapolation of Mass Flow Rate Calibration to Higher Levels of Mass Flow Rate

If mass flow rate encountered in an experiment exceeds values encompassed by the probe's calibration, a simple method can be applied to extrapolate the calibrations to higher levels of mass flow rate. Reference 4 showed how n, the exponent of Reynolds number in Eq. (9), for an individual sensor can be represented by the slope of a log Nu - log Re plot. The mass flow rate calibration parameter given by Eq. (26) is cast in a form which reflects the response of both sensors and is basically a Nusselt number term by virtue of Eqs. (2, 3, and 7). The parameter ψ is related to mass flow rate in Eq. (25) and ρu is directly proportional to Reynolds number. Therefore, an equivalent method of determining the value of n is to find the slope of a log ψ - log (ρu) plot, as shown in Fig. 7. This was done by using the values of ψ in Fig. 6 from the constant portions of the curves and the mass flow rates in Table 1. Values of ψ corresponding to the same angle of attack on the curve segments of nonzero slope could also have been used. The exponent was found to be equal to 0.75 over the range of conditions used for calibrating the hot-film probe. This is very close to the value of 0.72 determined for hot wires at similar flow conditions.[4] The exponent will not vary appreciably from its nominal value of 0.75 unless flow conditions are greatly different from those of the calibration. An extrapolation to mass flow rates three to four times greater than the calibrated values was necessary during the flowfield surveys for which this probe was used. This is only a moderate extension of the log ψ - log (ρu) plot, and the slope of 0.75 can be expected to provide a close approximation to the value of n at these higher levels of mass flow rate. The calibration data are extrapolated to include the experimental range of mass flow rate by using the equation

$$\psi_{exp} = \psi_{cal} [(\rho u)_{exp} / (\rho u)_{cal}]^{0.75} \quad (27)$$

as previously described. Figure 8 shows the extension of the calibration data for several angles of attack. Given a value of α from the calibration of ϕ vs α and a value of ψ, the mass flow rate can be determined by interpolation between the extrapolated curves.

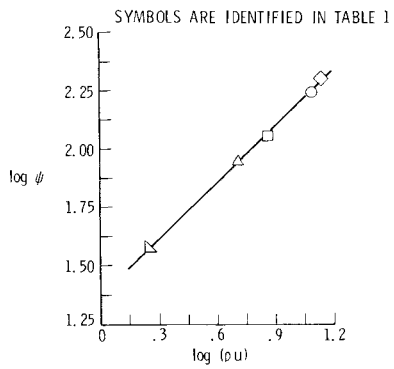

Fig. 7 Plot for determining the value of the exponent n.

Flowfield Surveys

Model and Tests

These data reduction techniques were applied to measurements obtained during surveys in the leeside flowfield of an early version of the Space Shuttle Orbiter shown in Fig. 9. The orifices are designated by numbers that were previously assigned during other wind-tunnel tests in which this model was used. The flowfield surveys discussed in this paper were initiated near these orifices. Measurements of flow angle and mass flow rate were made along paths beginning near the surface of the model and extending through the shock envelope and into the freestream. The tests were conducted at a freestream Mach number of 20.3, a freestream unit Reynolds number of $21.49 \times 10^6 m^{-1}$, a stagnation pressure of 6.90×10^6 N/m^2, and a stagnation temperature of 294 K. Surveys were made at both 10 and 30.3 deg angle of attack, but only representative samples of the data at $\alpha = 10$ deg will

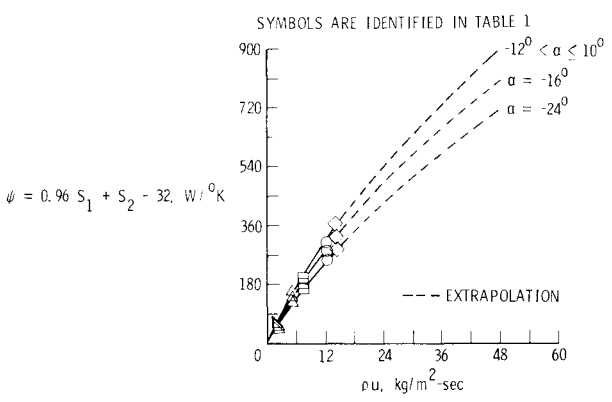

Fig. 8 Extension of mass flow rate calibration for various angles of attack.

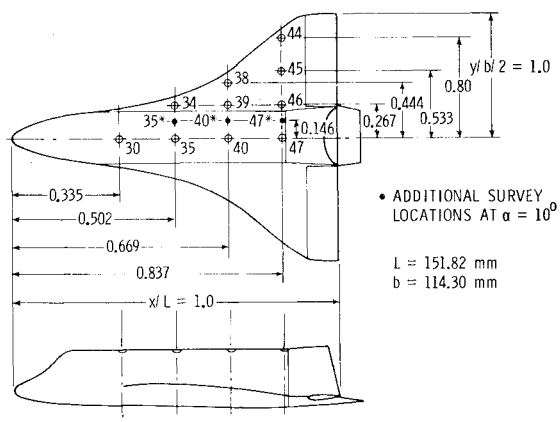

Fig. 9 Sketch of an early Space Shuttle Orbiter configuration.

be presented here. Reference 3 contains a complete discussion of both sets of data.

This investigation was designed to determine if flow patterns in the leeside flowfield of a shuttle configuration are adequately described by currently accepted leeside flow models. These models were developed from studies of oil flow patterns and heating contours on various space shuttle concepts and on simple geometries such as flat delta wings and cones. The familiar feather pattern observed in oil flows on the leeward centerline of space shuttle models is said to be caused by reattachment of flow associated with a system of vortices above the fuselage. A similar feather pattern on the side of the fuselage has been attributed to impingement of the shear layer that separates from the wing's top surface inboard of the leading edge. This produces a region of separated flow and a general circulatory pattern above the remainder of the wing's surface. This theory provides a plausible model of flow patterns in the shuttle's leeside flowfield, but it has never been proven by experimental data obtained in the flowfield away from a model's surface. Either hot-film or hot-wire probes are best suited to this task because of their fast response and high resolution. Use of the data reduction technique just described insures accurate flow angle and mass flow rate measurements over the wide range of flow conditions present in the leeside flowfield.

Experimental Data and Comparison with Theory

Figure 10 shows a typical set of flow angle measurements plotted as a function of distance from the surface of the model. The corresponding mass flow rate data are presented in Fig. 11. These measurements were made above the fuselage and a short distance outboard of the leeward symmetry plane near the aft end of the model at $\alpha = 10$ deg. The experimental results are compared with calculations for a series of points between the model and the shock that were provided by the supersonic three-dimensional external inviscid (STEIN) computer code.[10,11] The vertical angles in Fig. 10 were measured in a plane that is parallel to the symmetry plane and the crossflow angles were measured in a direction perpendicular to the symmetry plane. The hot-film probe is sensitive to flow properties in only one plane, which is represented by the plane of the paper in the side views of Fig. 1. In order to obtain both crossflow and vertical flow angle measurements, two surveys were made along each path through the flowfield. After making one set of measurements, the second survey was made with the probe rotated 90 deg about its axis. One sensor followed the other along the survey paths during the crossflow surveys so that each sensor occupied the same point in the flowfield, but at different times. The data were manipulated so that mass flow rates and crossflow angles were calculated using measurements made by both sensors at the same flowfield location, thus eliminating any error caused by the small separation between the sensing elements. Such a correction was not possible with the vertical flow angle measurements because the sensors were constantly separated by 0.5 mm at all points along the survey paths.

The sudden change in flow direction and the sharp peak in mass flow rate near $Z = 50$ mm in Figs. 10 and 11, respectively, mark the probe's passage through the bow shock and into the freestream. The extremely low mass flow rates out to $Z = 15$ mm in Fig. 11 indicate a region of separated flow. The initial peak in mass flow rate, near $Z = 25$ mm, is caused by a layer of high-density flow above the fuselage, which is a result of the bow shock impingement on the model's canopy.[3] The reversal in crossflow angles in Fig. 10 from outboard to inboard, with the accompanying changes in vertical angles, indicates the presence of a vortex within the separated region over the fuselage. This is in accordance with current leeside flow models. The experimental data and inviscid calculations

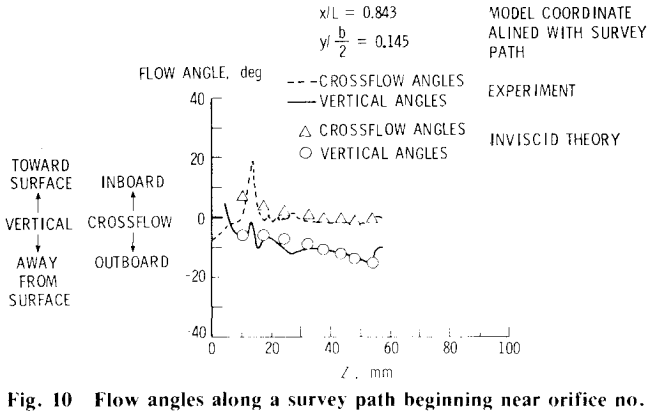

Fig. 10 Flow angles along a survey path beginning near orifice no. 47* at $\alpha = 10$ deg.

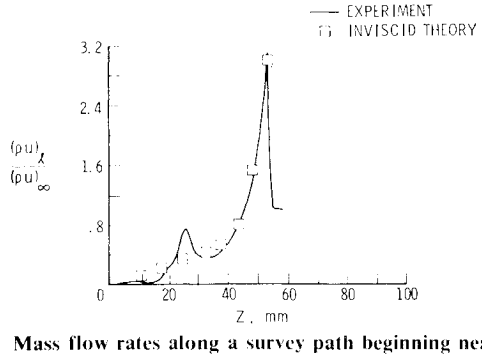

Fig. 11 Mass flow rates along a survey path beginning near orifice no. 47* at $\alpha = 10$ deg.

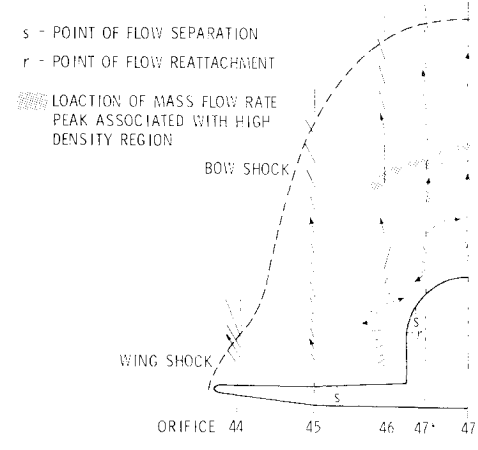

Fig. 12 Projection of flow direction vectors onto cross-sectional plane near $x/L = 0.837$ for $\alpha = 10$ deg.

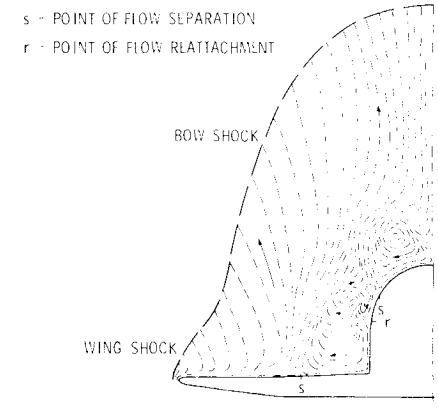

Fig. 13 Flow patterns derived from flow angle measurements near $x/L = 0.837$ at $\alpha = 10$ deg.

are in good agreement over approximately the outer half of the flowfield. This excludes the viscous layer surrounding the fuselage and the region influenced by the canopy shock impingement. Similar results were found at other locations above the fuselage and also along survey paths which traversed the separated region above the wing.

The flow angles measured along survey paths near the axial and semispan stations shown in Fig. 9 were used to compute the flow direction throughout most of the leeside flowfield. This is illustrated in Fig. 12 which shows the projection of flow direction vectors of unit length onto the cross-section plane at $x/L = 0.837$ at $\alpha = 10$ deg. The length and orientation of these projections gives an indication of the relative contribution of the crossflow and vertical components to the overall flow direction at each point on the survey paths. The locations of flow separation and reattachment on the model's surface, measured from oil flow photographs, are also indicated. The boundary of the shock envelope was determined by measurements from electron beam photographs and from the flowfield surveys. The shaded area above the fuselage represents the region in the flowf eld affected by the intial peak in mass flow rate that is associated with the canopy shock impingement. The vortices in the separated regions above the wing and fuselage are easily discerned with the data presented in this form. Note that inboard flow of the vortex over the wing is located too far above the model's surface to be directly involved with flow reattachment on the side of the fuselage. This is contrary to the currently accepted leeside flowfield models and indicates that a previously unrecognized mechanism is reponsible for flow reattachment near the aft end of this space shuttle configuration.

Figure 13 shows flow patterns derived from the flow angle measurements near $x/L = 0.837$ at $\alpha = 10$ deg. The drawing of this diagram was guided by the flow direction vectors in Fig. 12, as well as by photographs of oil flow patterns and the measured locations of flow separation and reattachment. The vortex above the fuselage develops as expected, based on accepted leeside flow models. Flow patterns in the separated region above the wing contradict these models because the patterns show that impingement of the shear layer is not the cause of flow reattachment on the side of the fuselage. The shear layer rises high above the wing as it rolls over toward the fuselage and a vortex forms directly under it. A consequence of this flow pattern is a pocket of reversed flow located close to the fuselage and above the reattachment line. It arises from interaction of downward flow in the vortex with upward flow on the side of the fuselage, and it may be a contributing factor to flow reattachment near the model's aft axial stations.

Concluding Remarks

A new data reduction technique for constant temperature hot-film and hot-wire probes has been presented which allows accurate measurement of flow angles and mass flow rate in an unknown flowfield. The calibration of a hot-film probe over a wide range of flow conditions and angles of attack at both supersonic and hypersonic velocities was used to demonstrate the procedure. It was shown that the probe's flow angle sensitivity could be made independent of Reynolds number effects by the proper choice of constants introduced into the equation for the flow angle calibration parameter. A simple method of extending a limited amount of mass flow rate calibration data to cover a wider range in angle of attack and to include higher levels of mass flow rate was also discussed.

The new technique was applied to data obtained using a hot-film probe during surveys in the leeside flowfield of a space shuttle configuration. The experimental measurements compare favorably with inviscid calculations provided by a three-dimensional flowfield program at locations outside of the viscous layer surrounding the fuselage. Flow patterns derived from flow angle measurements revealed an unexpectedly complex circulatory pattern in the separated region above the wing at aft axial stations on the model. These patterns show that currently accepted models of the shuttle's leeside flowfield are not universally applicable because flow reattachment on the side of the fuselage can be brought about by causes other than impingement of the shear layer.

References

[1]Arrington, J.P., Joiner, R.C., and Henderson, Jr., A., "Longitudinal Characteristics of Several Configurations at Hypersonic Mach Numbers in Conical and Contoured Nozzles," NASA TN D-2489, 1964.

[2]Weinstein, L.M., "A Shielded Fine-Wire Probe for Rapid Measurement of Total Temperature in High-Speed Flows," *Journal of Spacecraft and Rockets,* Vol. 8, April 1971, pp. 425-428.

[3]Helms, III, V.T., "Flow Angle and Mass Flow Rate Measurments in the Leeside Flowfield of a Space Shuttle Configuration," M.S. Thesis, George Washington University, Nov. 1977.

[4]Weinstein, L.M., "Effect of Oblique Shocks on Freestream Disturbances at $M_\infty \approx 20$ in Helium," M.S. Thesis, George Washington University, Feb. 1972.

[5]Olivari, D. and Borres, R., "Theory and Design of a Constant Temperature Linerarized Hot Wire Anemometer," von Karman Institute for Fluid Dynamics, Tech. Memo. 24, Oct. 1974.

[6]Kovasznay, L.S.C., "Hot Wire Method," in *Physical Measurments in Gas Dynamics and Combustion,* Vol. IX, Princeton University Press, Princeton, N.J., 1954, Art. F2.

[7]King, L.V., "On the Convection of Heat From Small Cylinders in a Stream of Fluid," *Philosophical Transactions of the Royal Society,* Sec. A. 214, Nov. 1914, pp. 373-432.

[8]Champagne, F.H., Sleicher, C.A., and Wehrmann, O.H., "Turbulence Measurements with Inclined Hot-Wires," *Journal of Fluid Mechanics,* Vol. 28, Part I, 1967.

[9]Jorgenson, F.E., DISA Inf. 11, 31., 1971.

[10]Marconi, F., Salas, M., and Yaeger, L., "Development of a Computer Code for Calculating the Steady Super/Hypersonic Inviscid Flow Around Real Configurations, Vol. I—Computational Technique," NASA CR-2675, April 1976.

[11]Marconi, F. and Yaeger, L., "Development of a Computer Code for Calculating the Steady Super/Hypersonic Inviscid Flow Around Real Configurations, Vol. II—Code Description," NASA CR-2676, May 1976.